IEEE Access
Multidisciplinary | Rapid Review | Open Access Journal

Received August 22, 2020, accepted September 16, 2020, date of publication September 25, 2020, date of current version October 7, 2020.

Digital Object Identifier 10.1109/ACCESS.2020.3026650

Transient Disturbances Based Non-Intrusive Ageing Condition Assessment for Cross-Bonded Cables

LULU LI, (Member, IEEE), ZONGYUN YANG, ZHAO LUO, (Member, IEEE), AND KEZHEN LIU
Faculty of Electric Power Engineering, Kunming University of Science and Technology, Kunming 650500, China

Corresponding author: Kezhen Liu (liukzh@foxmail.com)

This work was supported in part by the National Natural Science Foundation of China under Grant 52007079, in part by the Yunnan Provincial Talents Training Program under Grant KKSY201904011, and in part by the Scientific Research Foundation of Yunnan Provincial Department of Education under Grant 2020J0057.

ABSTRACT The cross-bonding is the most common shield/sheath-bonding system now in use on single-conductor shielded power cables for long distance power transmission. But the complex bonding brings great challenges to the assessment of cable ageing conditions. This paper proposes a non-intrusive ageing assessment method using the transient disturbances originating from the system. The cable relative permittivities, instead of the traditional dielectric loss angle, were extracted from the responses of the transient disturbances to character the ageing state more sensitively. The decoupling analysis of the cross-bonded cable and the corresponding relative permittivity identification model were investigated. Since the transient disturbances appear naturally and frequently, a continuous tracking of the cable ageing conditions can be established without interferences to the power system. Moreover, only the magnitudes rather than the phase angles of the cable currents/voltages are required in this method, which effectively simplifies the functions of the signal acquisition devices. The proposed method provides a new idea to assess the ageing conditions of the cross-bonded cables, and has the potential to be applied in industry.

INDEX TERMS Cross-bonded cable, ageing, transient disturbances, non-intrusive.

I. INTRODUCTION

The ageing condition of the power cables is always of concern to power industries [1]. If the assessment of the cable ageing conditions can be implemented non-intrusively, the outage caused by regular maintenance and even cable failure will be reduced greatly [2], [3].

Among the cables used in power systems, the cross-bonded cable is the most common installation method for long distance power transmission [4]. This kind of cable has the advantage of reducing the induced current for the cross connecting of the metallic shields. However, the complex connection also brings great challenges to the assessment of the ageing conditions for cross-bonded cables.

The ageing condition is used to describe the average deterioration degree of the entire cable insulation and can be usually represented by a certain insulation parameter, such as the widely accepted dielectric loss angle, i.e. tanδ. Until now, the off-line tanδ testing for power cables has been well developed, known as the very low-frequency tanδ test [5]–[7], but few studies had been done to apply it on-line for cross-bonded cables due to the practical difficulties. Pang *et al.* measured the tanδ by calculating the phase angle difference between the leakage current and the voltage at the mid-point of the cable [8]; Yang *et al.* distinguished the leakage currents from the sheath currents, and used the relative dielectric loss to determine the relative insulation condition of the cable [9]. However, the cross-bonding structure balances the vital leakage currents to near zero, which makes the implementations of these methods to the disadvantage. In addition, both the schemes demand very accurate synchronized phasor measurement at each terminal or joint of the cable. This may be costly for the installation of the cross-bonded cables.

In fact, the change of cable insulation condition will have little influence on the voltage/current phasors under 50/60Hz steady operation, whereas it may manifest itself in the transient waveforms more distinctly. This situation is even more pronounced on the cross-bonded cables. Fortunately, except

The associate editor coordinating the review of this manuscript and approving it for publication was Arpan Kumar Pradhan.

for the normal cases, the power system still has various natural transient disturbances, such as lightning, switch operations and faults [10], [11]. These disturbances, having sufficient magnitude and wide frequency band, can fully stimulate the cross-bonded cable to generate considerable transient responses containing a large amount of cable insulation information [12], [13]. More importantly, the transient responses are able to provide adequate amplitude data in frequency domain for insulation condition analysis, instead of using the phase angle information from GPS devices. These characteristics make the transient disturbance a potential solution for the non-intrusive ageing assessment of cross-bonded cables.

Recently, some preliminary studies have verified that the cable responses under transient disturbances contain the cable ageing conditions information. For instance, through simulation studies, [14] observed the behavior of the transient waveforms of the cable were significantly influenced by the cable insulation parameters. A neural network-based method that compared the frequency spectrum features of the transient voltages of the cables was proposed in [15], [16], and it successfully identified the aged cables from the new ones under capacitor switching. However, the cross-bonded cable is not included in these research studies, and the potential of the transient disturbances requires further investigation.

Based on above concerns and issues, using the system transient disturbances, this paper proposes a new method for non-intrusive ageing condition assessment of the cross-bonded cable. The cable relative permittivities, instead of the traditional dielectric loss angle, were extracted from the responses of the transient disturbances to character the ageing state more sensitively. Due to the characteristics of the natural transient disturbances, this method benefits the industry application as following:

1) A continuous tracking of cable ageing condition can be established with the constantly occurring of the transient disturbances.

2) No additional interferences will be introduced to the power system in operation.

3) The requirement of signal remote synchronization based on GPS is exempted because of the full use of the amplitude spectra of the transient waveforms.

The main idea of the proposed method is elaborated in Section II. And Section III investigates the decoupling solution of the cross-bonded cable model. The selection of the monitoring signals and frequency range for parameter extracting are presented in Section IV. Section V explains the extraction method of the relative permittivities and the corresponding assessment principle. Section VI uses case studies to verify the advantage of not requiring signal remote synchronization. Section VII concludes the paper.

II. THE NON-INTRUSIVE AGEING ASSESSMENT METHOD

This paper proposes to extract the cable insulation parameter from the responses under transient disturbances to achieve the non-intrusive ageing assessment. The relative permittivity is selected as cable insulation parameter, and the cable

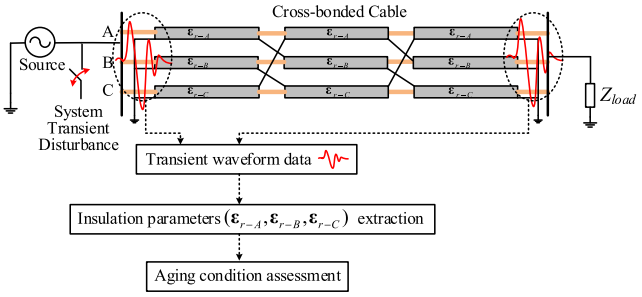

FIGURE 1. The idea of the proposed method.

responses are acquired at the both ends of the cross-bonded cable, as shown in Fig. 1. The cross-bonded cable system consists essentially in sectionalizing the metal shield into minor sections [4]. The relative permittivities (ε_{r-A}, ε_{r-B} and ε_{r-C} for phase A, B and C, respectively) of the XLPE insulation material of the cable can reflect the cable ageing conditions effectively [17]. The responses are excited by the transient disturbances generated from outside of the cable in the system, such as normal switching operations and various kinds of faults. Since the transient disturbances appear naturally and frequently in the power system, the successive comparison of the insulation parameters can be used to track the cable ageing conditions non-intrusively.

The extraction of the relative permittivities of the three phases of the cable is a specific parameter identification problem. It should solve two challenge problems: first, the cross-bonded structure should be decoupled to build the basic cable parameter equations; second, the signal data should be selected to support the parameter identification. The next two sections will address these problems, then the extraction model can be established.

III. THE DECOUPLING SOLUTION OF THE CROSS-BONDED CABLE MODEL

The cross-bonded cable model contains the desired insulation parameters. However, the cross-bonding structures complicate the extraction of the insulation parameters. Therefore, the decoupling of the cable model become the first step to solve this problem. This section will firstly introduce the cross-bonded cable model which can be used to analysis the transient responses under transient disturbances, and then deduces the decoupling solution.

A. THE CROSS-BONDED CABLE MODEL

The basic structure of the cross-bonded cable is the major section consisting of three minor sections per phase, as shown in Fig. 2 (a).

For the cable of each phase, three minor sections are separated, but each minor section can still be regarded as a continuous cable. Based on this, the distribution parameter model is adopted, as shown in Fig. 2 (b), taking Minor Section-A as an example. Additionally, to accurately obtain the transient response when transient disturbance occurs, the minor section

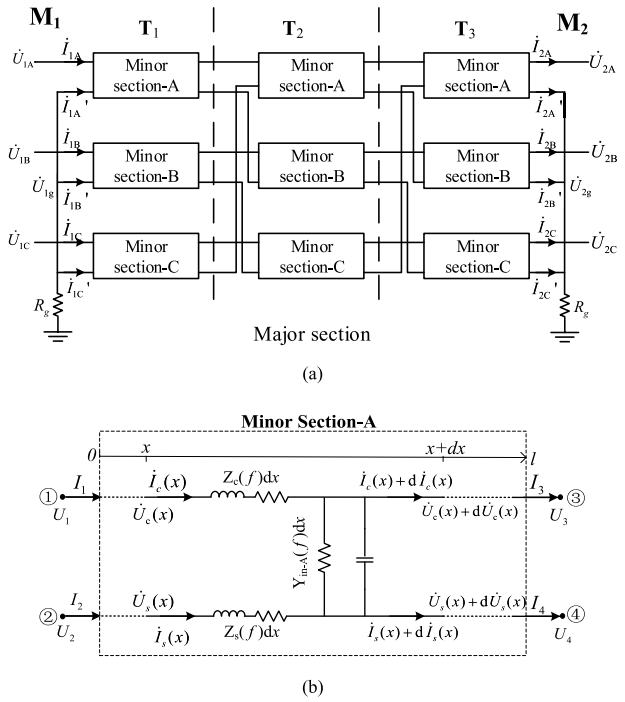

FIGURE 2. Frequency-dependent distributed cross-bonded cable model. (a) the basic structure of major section, (b) the minor section with frequency dependent parameters.

cable model uses the frequency-dependent parameters, and these parameters are calculated as follows [18]–[20]:

The frequency-dependent impedance of cable conductor per length:

$$Z_c(f) = \frac{1}{2\pi r_c}\sqrt{j2\pi f\mu_0\rho_c} + \frac{j2\pi f\mu_0}{2\pi}\ln\frac{r_s}{r_c} + \frac{1}{2\pi r_s}\sqrt{j2\pi f\mu_0\rho_s} \tag{1}$$

The frequency-dependent impedance of cable shield per length:

$$Z_s(f) = \frac{\rho_s}{\pi(r_s^2 - r_{in}^2)} + j2\pi f\left(-\frac{\mu_0}{2\pi}\left(\frac{r_s^2(r_s^2 - 2r_{in}^2)}{(r_s^2 - r_{in}^2)^2}\ln r_s + \frac{r_{in}^4}{(r_s^2 - r_{in}^2)^2}\ln r_x + \frac{r_{in}^2}{2(r_s^2 - r_{in}^2)}\right) + \frac{\mu_0}{8\pi}\right) \tag{2}$$

The frequency-dependent insulation admittance unit length:

$$Y_{in-A}(f) = j2\pi f\frac{2\pi}{\ln\frac{r_s}{r_c}}\varepsilon_0\cdot\varepsilon_{r-A} = j2\pi f\frac{2\pi}{\ln\frac{r_s}{r_c}}\varepsilon_0\cdot(\varepsilon'_{r-A} - j\varepsilon''_{r-A}) \tag{3}$$

where r_c, r_{in} and r_s are the equivalent radii of the cable conductor, insulation layer and metal shield, respectively; ρ_c and ρ_s are the specific resistivities of the cable conductor and metal shield; ε_0 is the permittivity of vacuum; μ_0 is the permeability of vacuum; and ε_{r-A} is the relative complex permittivity of cable in phase A, including the real part ε'_{r-A} and imaginary part ε''_{r-A}. ε_{r-A} is also frequency dependent.

The model and the corresponding parameters of Minor section-B and Minor section-C are similar to Minor section-A, except for the different insulation admittance $Y_{\text{in}-B}$ and $Y_{\text{in}-C}$ with different values of ε_{r-B} and ε_{r-C}, respectively.

B. THE DECOUPLING SOLUTION OF CABLE MODEL

The decoupling progress is to analyze the signal transmission in the cross-bonding structures, thus to build the connection of the measurements at the two ends of the cable. Because the cable model is composed of nine similar minor sections, the decoupling solution will derive from the analysis of Minor Section-A, then the complete solution of the major section will be deduced based on the cross connections between the minor sections.

1) FOR MINOR SECTION

As shown in Fig. 2 (b), when the transient responses are generated due to the transient disturbances, the frequency spectra of the currents and voltages on the cable conductors and shields can be obtained by Fast Fourier Transform (FFT). Then the following differential equations can be set up based on Kirchhoff's voltage and current laws:

$$\begin{cases} \dfrac{d\dot{I}_c(x)}{dx} = -Y_{in}(\dot{U}_c(x) - \dot{U}_s(x)) \\ \dfrac{d\dot{I}_s(x)}{dx} = Y_{in}(\dot{U}_c(x) - \dot{U}_s(x)) \\ \dfrac{d\dot{U}_c(x)}{dx} = -Z_c\dot{I}_c(x) \\ \dfrac{d\dot{U}_s(x)}{dx} = -Z_s\dot{I}_s(x) \end{cases} \tag{4}$$

where x is the distance from the head end of this minor section, $U_c(x)$, $I_c(x)$, $U_s(x)$ and $I_s(x)$ are the voltages and currents of the cable conductor and shield at distance x, respectively.

For simplicity, we define $\gamma = \sqrt{Y_{in}(Z_c + Z_s)}$ as the propagation coefficient, then the general solution of (4) can be obtained:

$$\begin{cases} \dot{I}_c(x) = C_1Z_s - C_2Z_s + C_3e^{\gamma x} - C_4e^{-\gamma x} \\ \dot{I}_s(x) = C_1Z_c - C_2Z_c - C_3e^{\gamma x} + C_4e^{-\gamma x} \\ \dot{U}_c(x) = C_1(1 - Z_cZ_sx) + C_2(1 + Z_cZ_sx) \\ \qquad -C_3Z_ce^{\gamma x}/\gamma - C_4Z_ce^{-\gamma x}/\gamma \\ \dot{U}_s(x) = C_1(1 - Z_cZ_sx) + C_2(1 + Z_cZ_sx) \\ \qquad +C_3Z_se^{\gamma x}/\gamma + C_4Z_se^{-\gamma x}/\gamma \end{cases} \tag{5}$$

where C_1, C_2, C_3 and C_4 are the unknown coefficients that need to be solved.

If the voltages and currents of the cable conductors and shields at the two ends of the minor section are represented by U_1, I_1, U_2, I_2 and U_3, I_3, U_4, I_4, respectively, as shown in Fig. 2 (b), then $C_1 \sim C_4$ in (5) can be solved. Finally, the connections between the measurements at the two ends

of this minor section can be established through the transfer function matrix **A**:

$$\begin{bmatrix} U_1 \\ I_1 \\ U_2 \\ I_2 \end{bmatrix} = \mathbf{A} * \begin{bmatrix} U_3 \\ I_3 \\ U_4 \\ I_4 \end{bmatrix} \tag{6}$$

where **A** is a 4×4 matrix, composed of 4 row vectors (see (7), as shown at the bottom of page).

The transfer function matrix of Minor section-B, expressed as **B,** and Minor section-C, expressed as **C**, are both similar to **A**, except for the different relative permittivities in the elements of $Y_{\text{in-B}}$ and $Y_{\text{in-C}}$.

2) FOR MAJOR SECTION

Combined with the transfer function matrix of each minor section, the decoupling solution of the cross-bonded cable model can be obtained by analysing the cross connections in the major section, as shown in Fig.2 (a).

We define the measurements at the two ends of the major section as $\mathbf{M}_1$ (left end) and $\mathbf{M}_2$ (right end):

$$\begin{cases} \mathbf{M}_1 = \left[U_{1\text{A}}\ I_{1\text{A}}\ U_{1g}\ I'_{1\text{A}}\ U_{1\text{B}}\ I_{1\text{B}}\ U_{1g} I'_{1B}\ U_{1\text{C}}\ I_{1\text{C}}\ U_{1g}\ I'_{1\text{C}}\right]^T \\ \mathbf{M}_2 = \left[U_{2\text{A}}\ I_{2\text{A}}\ U_{2g}\ I'_{2\text{A}}\ U_{2B}\ I_{2B}\ U_{2g}\ I'_{2B}\ U_{2\text{C}}\ I_{2\text{C}}\right. \\ \qquad \left. U_{2g}\ I'_{2\text{C}}\right]^T \end{cases} \tag{8}$$

where each measurement and the current set directions can be found in Fig.2 (a).

Then $\mathbf{M}_1$ and $\mathbf{M}_2$ can be connected by:

$$\mathbf{M}_1 = \mathbf{T}_1 * \mathbf{T}_2 * \mathbf{T}_3 * \mathbf{M}_2 \tag{9}$$

where $\mathbf{T}_1$, $\mathbf{T}_2$ and $\mathbf{T}_3$ are the transfer matrixes of the three groups of the minor sections, as marked in Fig. 2 (a). And they depend on the cross connections with the exchange of the shield voltages and currents.

For $\mathbf{T}_1$, no cross connections are included, so its expression is (10), as shown at the bottom of the next page.

For $\mathbf{T}_2$ and $\mathbf{T}_3$, the cross-bonding makes the current and voltage of the metal shield of each phase change to that of the other phase sequentially, i.e. Phase A to Phase B, Phase B to Phase C, and Phase C to Phase A. Thus, $\mathbf{T}_2$ and $\mathbf{T}_3$ are transformed to (11), as shown at the bottom of the next page.

The complete solution of the cross-bonded cable can be obtained by substituting (10) and (11) to (9). Then the unknown relative permittivities (ε_{r-A}, ε_{r-B} and ε_{r-C}) can be extracted through the equations established in (12), which can fully use the amplitude spectra of the transient measurement waveforms to avoid the phase angle calculation.

$$|\mathbf{M}_1| = |\mathbf{T}_1 * \mathbf{T}_2 * \mathbf{T}_3 * \mathbf{M}_2| \tag{12}$$

IV. SELECTION OF THE MONITORING SIGNALS AND FREQUENCY RANGE

The extraction of the relative permittivities can be realized by the parameter identification algorithm. However, as shown in (12), a large number of optimal equations can be established in frequency domain with different measurements at different frequency points. Obviously, not every measurement at every frequency is sensitive to the change of the relative permittivity. To aid the optimal solution, the sensitivity analysis is conducted to select the suitable monitoring signals and frequency range, then the objective function can be built and solved.

The selection of the monitoring signals and frequency range are based on the frequency-domain sensitivity analysis. The frequency-domain sensitivity reflects the contribution of the unknown parameters to the change of the objective function at each frequency point. The larger the sensitivity is, the easier the parameters can be identified using this data. According to this, the suitable monitoring signals and frequency can be determined.

For the complexity of the matrix in (12) which including (10) and (11), this paper uses a model-based method to calculate the frequency-domain sensitivity. The signals in $|\mathbf{M}_2|$ are assumed as the measurement signals, whereas that in $|\mathbf{M}_1|$ are regarded as the observed signals, then the frequency-domain sensitivities can be calculated by (13) and (14), as shown at the bottom of the next page, where $S_{\varepsilon'_{\mathbf{r}-x}}(f)$ and $S_{\varepsilon''_{\mathbf{r}-x}}(f)$ are the frequency-domain sensitivities of the signals in

$$\mathbf{A} = \begin{bmatrix} A_{11} & A_{12} & A_{13} & A_{14} \\ A_{21} & A_{22} & A_{23} & A_{24} \\ A_{31} & A_{32} & A_{33} & A_{34} \\ A_{41} & A_{42} & A_{43} & A_{44} \end{bmatrix}$$
$$= \frac{1}{2(z_c + z_s)} \begin{bmatrix} z_c(e^{\gamma l} + e^{-\gamma l}) + 2z_s & \frac{z_c^2}{\gamma}(e^{\gamma l} - e^{-\gamma l}) + 2z_c z_s l & -z_c(e^{\gamma l} + e^{-\gamma l}) + 2z_c & -\frac{z_c z_s}{\gamma}(e^{\gamma l} - e^{-\gamma l}) + 2z_c z_s l \\ \gamma(e^{\gamma l} - e^{-\gamma l}) & z_c(e^{\gamma l} + e^{-\gamma l}) + 2z_s & -\gamma(e^{\gamma l} - e^{-\gamma l}) & -z_s(e^{\gamma l} + e^{-\gamma l}) + 2z_s \\ -z_s(e^{\gamma l} + e^{-\gamma l}) + 2z_s & -\frac{z_c z_s}{\gamma}(e^{\gamma l} - e^{-\gamma l}) - 2z_c z_s l & z_s(e^{\gamma l} + e^{-\gamma l}) + 2z_c & \frac{z_s^2}{\gamma}(e^{\gamma l} - e^{-\gamma l}) - 2z_c z_s l \\ -\gamma(e^{\gamma l} - e^{-\gamma l}) & -z_c(e^{\gamma l} + e^{-\gamma l}) + 2z_c & \gamma(e^{\gamma l} - e^{-\gamma l}) & z_s(e^{\gamma l} + e^{-\gamma l}) + 2z_c \end{bmatrix} \tag{7}$$

$\mathbf{M}_1$ respect to the real part and the imaginary part of the relative permittivity of phase X (can be A, B or C), respectively. $|\mathbf{M}_{1-0}|$ is the amplitude spectrum matrix of the observed signals with initial parameters; $|\mathbf{M}_{1-\Delta}|$ is the amplitude spectrum matrix of the observed signals under the updated parameters with a tiny increment Δ, where Δ is selected as the empirical value of 1% by trial-and-error method.

To illustrate the calculation progress, a typical 110kV cross-bonded cable is used as an example. The cables in three phases are set at three different ageing levels, and the parameters are listed in Table 1.

The calculated frequency-domain sensitivities are shown in Fig. 3. The monitoring signals and frequency range which own large frequency sensitivities will be selected for parameter identification. From the sensitivity curves as shown in this figure, according to the selection principle and considering this method will extract the relative permittivities of the three phases at the same time, the selected monitoring signals are exhibited in (15), and the frequency range is selected as 10∼15kHz.

$$\mathbf{M}_{1-\text{select}} = [\, I_{1\text{A}} \quad I'_{1\text{A}} \quad I_{1\text{B}} \quad I'_{1\text{B}} \quad I_{1\text{C}} \quad I'_{1\text{C}} \,]^T \tag{15}$$

TABLE 1. The cable parameters.

Symbol	Description	Value
U_n	rated voltage	110kV
l	length	480*3m
r_c, r_{in}, r_s,	equivalent radii	17, 35.2, 36.2mm
ρ_c / ρ_s	specific resistivity	1.75e-8 Ω·m
ε_{r-A}	light ageing	2.57-j0.00512
ε_{r-B}	moderate ageing	2.64- j0.0211
ε_{r-C}	severe ageing	2.70-j0.0555

V. EXTRACTION OF THE RELATIVE PERMITTIVITY AND AGEING ASSESSMENT

A. IDENTIFICATION OF THE RELATIVE PERMITTIVITY BASED ON DE ALGORITHME

Based on the selection results of the monitoring signals and frequency range above, the objective function can be established. Firstly, we define the desired parameters of three

$$\mathbf{T}_1 = \begin{bmatrix} A_{11} & A_{12} & A_{13} & A_{14} & 0 & \dots & 0 & 0 & \dots & 0 \\ A_{21} & A_{22} & A_{23} & A_{24} & \vdots & \ddots & \vdots & \vdots & \ddots & \vdots \\ A_{31} & A_{32} & A_{33} & A_{34} & & & & & & \\ A_{41} & A_{41} & A_{41} & A_{41} & 0 & \dots & 0 & 0 & \dots & 0 \\ 0 & \dots & 0 & B_{11} & B_{12} & B_{13} & B_{14} & 0 & \dots & 0 \\ \vdots & \ddots & \vdots & B_{21} & B_{22} & B_{23} & B_{24} & \vdots & \ddots & \vdots \\ & & & B_{31} & B_{32} & B_{33} & B_{34} & & & \\ 0 & \dots & 0 & B_{41} & B_{42} & B_{43} & B_{44} & 0 & \dots & 0 \\ 0 & \dots & 0 & 0 & \dots & 0 & C_{11} & C_{12} & C_{13} & C_{14} \\ \vdots & \ddots & \vdots & \vdots & \ddots & \vdots & C_{21} & C_{22} & C_{23} & C_{24} \\ & & & & & & C_{31} & C_{32} & C_{33} & C_{34} \\ 0 & \dots & 0 & 0 & \dots & 0 & C_{41} & C_{42} & C_{43} & C_{44} \end{bmatrix} \tag{10}$$

$$\mathbf{T}_2 = \mathbf{T}_3 = \begin{bmatrix} A_{11} & A_{12} & A_{13} & A_{14} & 0 & \dots & 0 & 0 & \dots & 0 \\ A_{21} & A_{22} & A_{23} & A_{24} & 0 & \dots & 0 & 0 & \dots & 0 \\ 0 & \dots & 0 & B_{31} & B_{32} & B_{33} & B_{34} & 0 & \dots & 0 \\ \vdots & \ddots & \vdots & B_{41} & B_{42} & B_{43} & B_{44} & \vdots & \ddots & \vdots \\ & & & B_{11} & B_{12} & B_{13} & B_{14} & & & \\ 0 & \dots & 0 & B_{21} & B_{22} & B_{23} & B_{24} & 0 & \dots & 0 \\ 0 & \dots & 0 & 0 & \dots & 0 & C_{31} & C_{32} & C_{33} & C_{34} \\ \vdots & \ddots & \vdots & \vdots & \ddots & \vdots & C_{41} & C_{42} & C_{43} & C_{44} \\ & & & & & & C_{11} & C_{12} & C_{13} & C_{14} \\ 0 & \dots & 0 & 0 & \dots & 0 & C_{21} & C_{22} & C_{23} & C_{24} \\ A_{31} & A_{32} & A_{33} & A_{34} & 0 & \dots & 0 & 0 & \dots & 0 \\ A_{41} & A_{41} & A_{41} & A_{41} & 0 & \dots & 0 & 0 & \dots & 0 \end{bmatrix} \tag{11}$$

$$S_{\varepsilon'_{\mathbf{r}-x}}(f) = \frac{\left|\mathbf{M}_{1-\Delta}((\varepsilon'_{\mathbf{r}-x} + \Delta\varepsilon'_{r-x}) - j\cdot\varepsilon''_{\mathbf{r}-x})\right| - \left|\mathbf{M}_{1-0}(\varepsilon'_{\mathbf{r}-x} - j\cdot\varepsilon''_{\mathbf{r}-x})\right|}{\Delta\varepsilon'_{r-x}} \tag{13}$$

$$S_{\varepsilon''_{\mathbf{r}-x}}(f) = \frac{\left|\mathbf{M}_{1-\Delta}(\varepsilon'_{\mathbf{r}-x} - j\cdot(\varepsilon''_{\mathbf{r}-x} + \Delta\varepsilon''_{r-x}))\right| - \left|\mathbf{M}_{1-0}(\varepsilon'_{\mathbf{r}-x} - j\cdot\varepsilon''_{\mathbf{r}-x})\right|}{\Delta\varepsilon''_{r-x}} \tag{14}$$

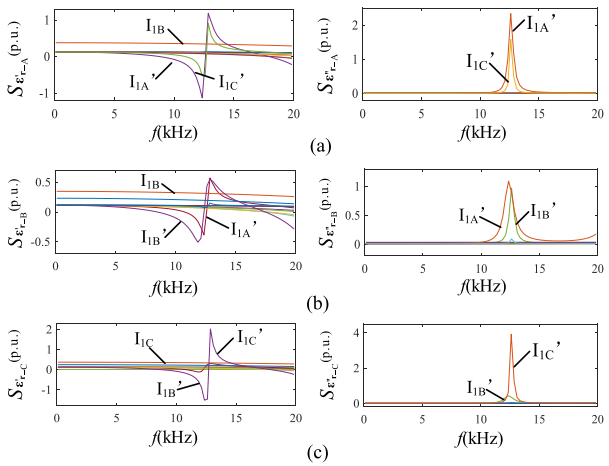

FIGURE 3. The frequency-domain sensitivity of the relative permittivity of (a) phase A, (b) phase B, and (c) phase C.

phases as

$$\varepsilon_{\mathbf{r}} = \left[\varepsilon'_{r-A}, \varepsilon''_{r-A}, \varepsilon'_{r-B}, \varepsilon''_{r-B}, \varepsilon'_{r-C}, \varepsilon''_{r-C}\right]^T \tag{16}$$

By using the solution of the cross-bonded cable model in (12) with selected signals in (15), the optimization problem can be written as following:

$$\begin{aligned}
\hat{\varepsilon}_{\mathbf{r}} &= \arg\min_{\varepsilon_{\mathbf{r}}} f(\varepsilon_{\mathbf{r}}) \\
f(\varepsilon_{\mathbf{r}}) &= \sum_{\mathbf{f=10kHz}}^{\mathbf{15kH}} \left[\left|\hat{\mathbf{M}}_{\mathbf{1-select}}(\varepsilon_{\mathbf{r}})\right| - \left|\mathbf{M}_{\mathbf{1-select}}\right|\right]^{\mathbf{2}} \\
\left|\hat{\mathbf{M}}_{\mathbf{1-select}}(\varepsilon_{\mathbf{r}})\right| &= \left|[\mathbf{T(2},:),\mathbf{T(4},:),\mathbf{T(6},:),\mathbf{T(8},:),\mathbf{T(10},:),\right. \\
&\qquad \left.\mathbf{T(12},:),]^{\mathbf{T}} * M_{\mathbf{2}}\right| \\
\mathbf{T} &= \mathbf{T_1}(\varepsilon_{\mathbf{r}}) * \mathbf{T_2}(\varepsilon_{\mathbf{r}}) * \mathbf{T_3}(\varepsilon_{\mathbf{r}})
\end{aligned} \tag{17}$$

where $\left|\hat{\mathbf{M}}_{1-select}\right|$ is the estimation function matrix of $|\mathbf{M}_{1-select}|$, and it can be calculated by the measurements in $\mathbf{M}_2$ and the transfer matrix $\mathbf{T}$. Here $\mathbf{T}$(n,:) represents the n^{th} row of matrix $\mathbf{T}$, which relates to the corresponding selected signal.

The objective function (17) is actually a multi-objective, multi-parameter and highly nonlinear optimization problem. This paper uses the DE (Differential Evolution) algorithm which can handle this complex and large-scale optimization problem [21]. This algorithm also has quick convergence, robustness and capability of searching the global optimal solution. The main calculation processes are shown in Fig. 4.

The searching processes are similar to the steps employed by a standard evolutionary algorithm, but the variants perturb the current-generation population members with the scaled difference of randomly selected and distinct population members. The mutation and crossover are controlled by the parameters cr and F, respectively, as shown in Fig. 4. The best-suited relative permittivities can be found once the fitting error is below the setting termination value.

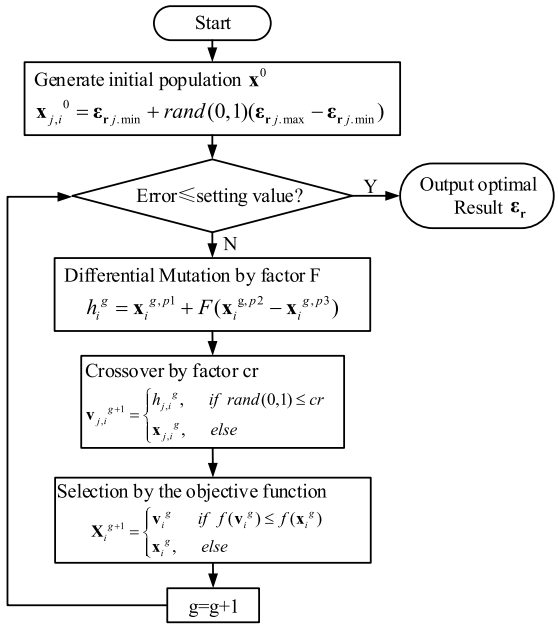

FIGURE 4. Flow chart of the optimal progress to identify the relative permittivities.

B. THE AGEING CONDITION ASSESSMENT METHOD

Once the relative permittivities of each phase are identified, the ageing condition can be non-intrusively assessed by comparing the calculation results with the pre-defined values. This paper adopts the reference values as shown in Table 2 [18]. Note that the relative permittivity is actually frequency dependent as stated earlier. However, the variation of its value is negligible at the kHz level [22]. The data measured among several kHz ranges can be considered as referring to a constant relative permittivity. Therefore, the reference values in this table are formulated for kHz frequency range use which is specially for transient disturbance analysis.

TABLE 2. The reference values for cable ageing assessment.

Ageing conditions	Relative permittivity ($\varepsilon_r' - j\varepsilon_r''$)
intact	<2.52-j**0.0025**
light ageing	2.52-j**0.0025**~2.60-j**0.013**
moderate ageing	2.60-j**0.013**~2.66-j**0.0266**
severe ageing	>2.66-j**0.0266**

A notable observation made from Table 2 is that the imaginary parts of the relative permittivities have a difference in the order of magnitude, which can distinctly reflect the ageing condition of cable. Therefore, this paper takes the imaginary part of the insulation parameter as the main criteria for ageing assessment. The effectiveness will be tested in the next section.

VI. CASE STUDY

Three cable ageing cases with three typical kinds of system transient disturbances are simulated to validate the proposed method. To test the advantage of this method of not requiring remote synchronization based on GPS, the measurements at the two ends of the cross-bonded cable are intentionally asynchronously sampled. The influence of signal noise on the ageing assessment results are discussed at the end of this section.

A. TEST SYSTEM

The test system in Fig. 5 including cross-bonded cable will be used for the simulations in EMTP/ATP software. The ageing conditions of the three phases of the cross-bonded cable are set at three different ageing levels: phase A-light ageing, phase B-moderate ageing and phase C-severe ageing. The cable parameters are calculated by (1)-(3) using the values listed in Table 1. The frequency-dependent characteristic of the cable is modelled by the Vector-Fitting method as introduced in the Appendix. The parameters of the system and the three transient disturbances are shown in Table 3 and Table 4, respectively.

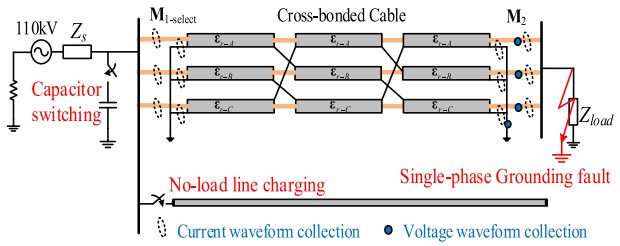

FIGURE 5. Test system.

TABLE 3. The system parameters.

Symbol	Description	Value
V_s	system voltage	110kV
Z_s	system impedance	1.936+j6.292Ω
R_s	system grounding resistance	2Ω
Z_{load}	three phase loads	300+j400Ω

TABLE 4. The transient disturbance parameters.

Types	Description
capacitor switching	capacity: 35.27Mvar
single-phase grounding fault	fault phase: C fault resistance: 10Ω
no-load line charging	1000m with parameters as same as Table I

B. TRANSIENT RESPONSE WAVEFORMS UNDER THE THREE CASES

When the three transient disturbances occur, the cable transient response waveforms and the corresponding amplitude spectra are shown in Fig. 6 ∼ Fig. 8 (for space limitation, only the signals in $\mathbf{M}_{1-select}$ and the cable conductor voltages in $\mathbf{M_2}$ are presented).

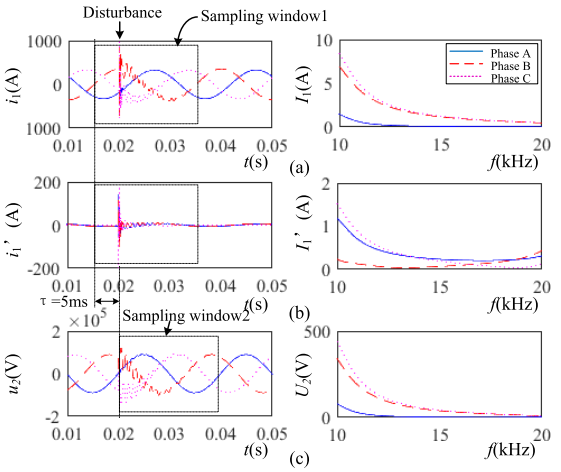

FIGURE 6. The transient responses (left) and amplitude spectra (right) under capacitor switching. (a) cable conductor currents, (b) cable shield currents, and (c) cable conductor voltages.

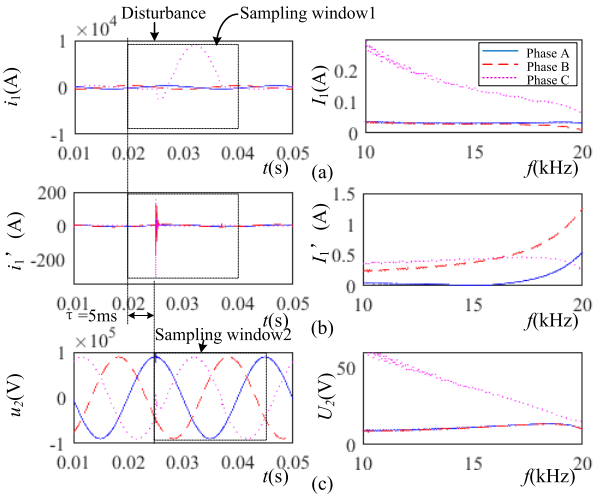

FIGURE 7. The transient responses (left) and amplitude spectra (right) under grounding fault. (a) cable conductor currents, (b) cable shield currents, and (c) cable conductor voltages.

The curves in these figures show that all the transient responses under the three typical transient disturbances have large waveform distortions, and can be detected and extracted easily by the methods in the field of power quality analysis [23], [24]. Additionally, note that, because of the cross-bonding of the shields, every response signal will contain the insulation information of all the three phases; thus, from Fig. 6 ∼ Fig. 8, the frequency spectra under the three kinds of disturbances can provide sufficient magnitude to identify the relative permittivities.

C. AGEING ASSESSMENT RESULTS UNDER ASYNCHRONOUS SAMPLING

To validate the advantage of the proposed method, i.e. not requiring remote synchronization based on GPS,

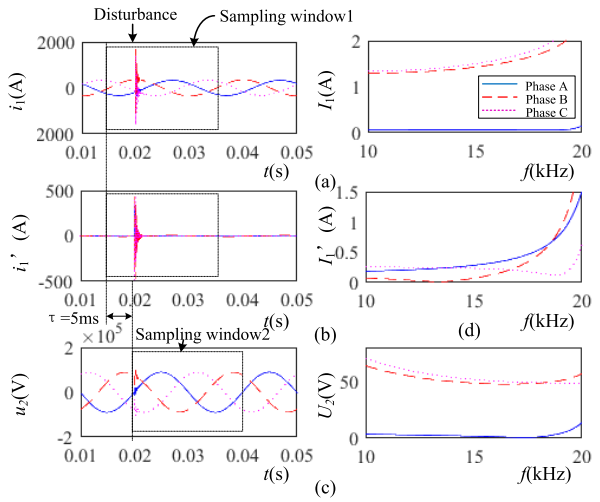

FIGURE 8. The transient responses (left) and amplitude spectra (right) under no-load line charging. (a) cable conductor currents, (b) cable shield currents, and (c) cable conductor voltages.

an intentional time deviation ($\tau = 5ms$) is set between the sampling windows at the two terminations of the cable, as shown in Fig. 6 ∼ Fig. 8.

Using the parameter extraction method presented in Section V, the relative permittivities can be estimated and used for ageing assessment. The calculation values and the assessment results are shown in Fig. 9 for the three transient disturbance cases.

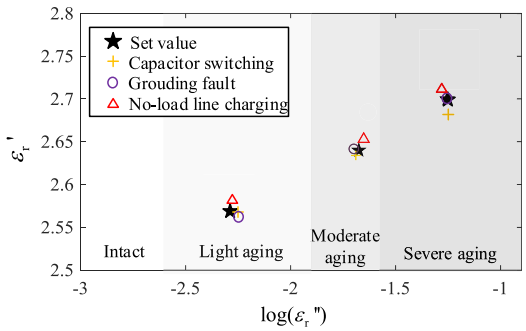

FIGURE 9. The estimated relative permittivities and ageing assessment results under asynchrony sampling.

Fig. 9 shows, even if a considerable time deviation (5ms) exists between the signal sampling windows at the two terminations of the cable, the relative permittivities still can be estimated accurately. The proposed method can work effectively without the need of remote signal synchronization. A correct index also can be observed from this figure, and the clear distinction among the imaginary parts of the estimated relative permittivities can easily help engineers to make a decision for the maintenance or the replacement of the aged cables.

D. AGEING ASSESSMENT RESULTS WHEN CONSIDERING SIGNAL NOISE

To further test the anti-noise ability of the proposed method, two cases with SNR = 50 and SNR = 60 are recalculated applying the relative permittivity identification algorithm. The results are shown in Fig. 10 (a) and Fig. 10 (b), respectively.

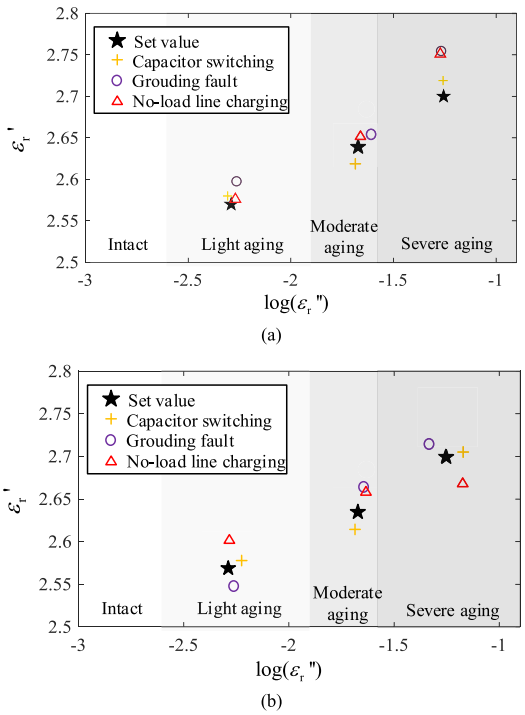

FIGURE 10. The estimated relative permittivities and ageing assessment results when considering noise. (a) SNR = 50, (b) SNR = 60.

From the new estimation values, some errors can be expected compared with the results in Fig. 9. Because the value ranges of the real parts are insensitive to the change of the cable ageing conditions, their calculation values have relatively larger errors than the imaginary parts. However, as mentioned before, the determinant of the ageing condition, i.e. the imaginary part, still maintains considerable accuracy. And an obvious difference of the estimated imaginary parts can be observed in Fig. 10 (a) and Fig. 10 (b), which implies the proposed method is able to give reliable assessment advice even the measurement signals contain some noise.

VII. CONCLUSION

This paper utilizes the transient disturbances in the power system to non-intrusively assess the ageing conditions of the cross-bonded cables. The cable relative permittivities were extracted to get the cable ageing conditions. The decoupling of the cross-bonded structure was conducted to build the relative permittivity identification model. Through sensitive analyses for a typical 110kV XLPE cable, the currents on cable conductors and shields with frequency range of 10-15 kHz were found to be the contribution data to

the identification. Three transient disturbances in the power system were simulated to verify the proposed method. The results show that, the transient disturbances can stimulate the cross-bonded cable generating considerable transient responses, and this method can effectively reveal the ageing conditions without the need of any remote signal synchronization.

APPENDIX

The Vector-Fitting [25] method used for modelling the frequency-dependent characteristics of the cable is explained below.

Because the expressions of (1) ∼ (3) are too complex to model in the simulation software by conventional methods, we use the Vector-Fitting method to transfer them into rational fractions as follows:

$$F(\omega) = j\omega \sum_{i=1}^{n} \frac{c_i}{j\omega - a_i} + j\omega h + d \tag{18}$$

where c_i and a_i are the residue and pole, respectively, and can be real or complex conjugate; n represents the order depending on the desired fitting accuracy; h and d are real numbers.

Based on the fitting results obtained by (18), which are actually another forms of (1) ∼ (3), the frequency-dependent characteristics of cables can be easily modelled by the cascaded circuits [26]. The cascaded circuits including the series impedance and shunt admittance are shown in Fig. 11.

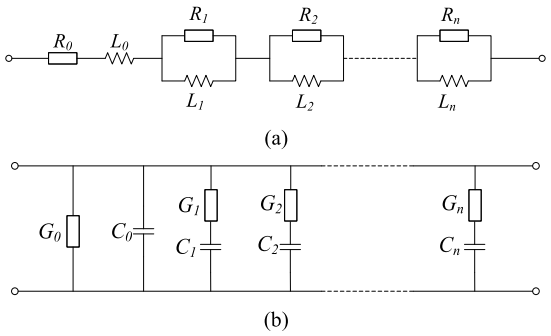

FIGURE 11. Frequency-dependent cable model. (a) series impedance equivalent circuit per unit, (b) shunt admittance equivalent circuit per unit.

In these cascaded circuits, R, L, G and C are all calculated by the fitting parameters in (18). The number n in the circuits is the same as the order n in (18). In this paper, n is selected as 3, which is enough to model the frequency-dependent characteristics of the cable parameters for analysis. The fitting results under each ageing condition are shown in Table 5 and Table 6.

TABLE 5. The system parameters.

Symbol	Value	Symbol	Value
$R_0(\Omega)$	3.8358e-04	L_0(H)	2.9246e-05
$R_1(\Omega)$	0.2585	L_1(H)	2.3468e-07
$R_2(\Omega)$	0.0839	L_2(H)	3.2105e-07
$R_3(\Omega)$	0.0467	L_3(H)	6.3098e-07

TABLE 6. The system parameters.

Symbol	Value	Symbol	Value
light ageing			
G_0(S)	4.6134e-10	$C_0(\Omega)$	1.8806e-10
G_1(S)	1.6280e-07	$C_1(\Omega)$	6.2337e-14
G_2(S)	1.8329e-08	$C_2(\Omega)$	4.0172e-14
G_3(S)	4.3722e-09	$C_3(\Omega)$	5.4989e-14
moderate ageing			
G_0(S)	4.4358e-09	$C_0(\Omega)$	1.9483e-10
G_1(S)	1.6056e-06	$C_1(\Omega)$	6.1078e-13
G_2(S)	1.7866e-07	$C_2(\Omega)$	3.8946e-13
G_3(S)	4.2373e-08	$C_3(\Omega)$	5.2884e-13
severe ageing			
G_0(S)	1.8255e-08	$C_0(\Omega)$	1.9597e-10
G1(S)	6.9860e-06	C1(Ω)	2.6206e-12
G2(S)	7.5825e-07	C2(Ω)	1.6335e-12
G3(S)	1.7757e-07	C3(Ω)	2.1789e-12

REFERENCES

[1] K. Kopsidas and S. Liu, "Power network reliability framework for integrating cable design and ageing," *IEEE Trans. Power Syst.*, vol. 33, no. 2, pp. 1521–1532, Mar. 2018.

[2] S. V. Suraci, D. Fabiani, A. Xu, S. Roland, and X. Colin, "Ageing assessment of XLPE LV cables for nuclear applications through physico-chemical and electrical measurements," *IEEE Access*, vol. 8, pp. 27086–27096, 2020.

[3] G. Ye, H. Li, F. Lin, J. Tong, X. Wu, and Z. Huang, "Condition assessment of XLPE insulated cables based on polarization/depolarization current method," *IEEE Trans. Dielectr. Electr. Insul.*, vol. 23, no. 2, pp. 721–729, Apr. 2016.

[4] *IEEE Guide for Bonding Shields and Sheaths of Single-Conductor Power Cables Rated 5 kV through 500 kV*, IEEE Standard 575-2014, 2014.

[5] J. C. Hernandez-mejia, R. Harley, N. Hampton, and R. Hartlein, "Characterization of ageing for MV power cables using low frequency tan δ diagnostic measurements," *IEEE Trans. Dielectr. Electr. Insul.*, vol. 16, no. 3, pp. 862–870, Jun. 2009.

[6] Y. Liu and X. Cao, "Insulation performance evaluation of HV AC/DC XLPE cables by 0.1 Hz tan δ test on circumferentially peeled samples," *IEEE Trans. Dielectr. Electr. Insul.*, vol. 24, no. 6, pp. 3941–3950, Dec. 2017.

[7] *IEEE Guide for Field Testing of Shielded Power Cable Systems Using Very Low Frequency (VLF) (less than 1 Hz)*, IEEE Standard 400.2-2013, 2013.

[8] B. Pang, B. Zhu, X. Wei, S. Wang, and R. Li, "On-line monitoring method for long distance power cable insulation," *IEEE Trans. Dielectr. Electr. Insul.*, vol. 23, no. 1, pp. 70–76, Feb. 2016.

[9] Y. Yang, D. M. Hepburn, C. Zhou, W. Zhou, and Y. Bao, "On-line monitoring of relative dielectric losses in cross-bonded cables using sheath currents," *IEEE Trans. Dielectr. Electr. Insul.*, vol. 24, no. 5, pp. 2677–2685, Oct. 2017.

[10] Y.-J. Shin, E. J. Powers, M. Grady, and A. Arapostathis, "Power quality indices for transient disturbances," *IEEE Trans. Power Del.*, vol. 21, no. 1, pp. 253–261, Jan. 2006.

[11] T. Zhong, S. Zhang, G. Cai, Y. Li, B. Yang, and Y. Chen, "Power quality disturbance recognition based on multiresolution S-Transform and decision tree," *IEEE Access*, vol. 7, pp. 88380–88392, 2019.

[12] D. Salles and W. Xu, "Information extraction from PQ disturbances—An emerging direction of power quality research," in *Proc. IEEE 15th Int. Conf. Harmon. Qual. Power*, Jun. 2012, pp. 649–655.
[13] B. D. Russell and C. L. Benner, "Intelligent systems for improved reliability and failure diagnosis in distribution systems," *IEEE Trans. Smart Grid*, vol. 1, no. 1, pp. 48–56, Jun. 2010.
[14] F. N. Fessol, A. Mohd Ariffin, and H. A. Illias, "Influence of underground cable insulation parameters on transient overvoltages," in *Proc. IEEE 7th Int. Power Eng. Optim. Conf. (PEOCO)*, Jun. 2013, pp. 362–365.
[15] B. Pushpanathan and S. Grzybowski, "Analysis of online capacitor switching transient voltages on experimental MV cables," in *Proc. Int. Conf. High Voltage Eng. Appl. (ICHVE)*, Sep. 2014, pp. 1–4.
[16] B. Pushpanathan, S. Grzybowski, and T. O. Bialek, "Identification of aged cable section in 12.5 kV URD system based on frequency spectrum," in *Proc. PES T D*, May 2012, pp. 1–5.
[17] G. Mugala, R. Eriksson, and P. Pettersson, "High frequency characteristics of water-tree degraded XLPE insulation in power cables," *IEEE Trans. Dielectr. Electr. Insul.*, vol. 14, no. 5, pp. 1271–1277, Oct. 2007.
[18] Z. Zhou, D. Zhang, J. He, and M. Li, "Local degradation diagnosis for cable insulation based on broadband impedance spectroscopy," *IEEE Trans. Dielectr. Electr. Insul.*, vol. 22, no. 4, pp. 2097–2107, Aug. 2015.
[19] G. Mugala, R. Eriksson, and P. Pettersson, "Dependence of XLPE insulated power cable wave propagation characteristics on design parameters," *IEEE Trans. Dielectr. Electr. Insul.*, vol. 14, no. 2, pp. 393–399, Apr. 2007.
[20] T. Aloui, F. B. Amar, and H. H. Abdallah, "Fault prelocalization of underground single-phase cables: Modeling and simulation," *Int. J. Electr. Power Energy Syst.*, vol. 44, no. 1, pp. 514–519, Jan. 2013.
[21] S. Das and P. N. Suganthan, "Differential evolution: A survey of the State-of-the-Art," *IEEE Trans. Evol. Comput.*, vol. 15, no. 1, pp. 4–31, Feb. 2011.
[22] J. Yang, R. Huang, and D. Zhang, "A field-circuit coupled method to accurately determine intrinsic complex permittivity of XLPE insulation material," *IEEE Trans. Dielectr. Electr. Insul.*, vol. 15, no. 2, pp. 334–341, Apr. 2008.
[23] C. A. G. Marques, D. D. Ferreira, L. R. Freitas, C. A. Duque, and M. V. Ribeiro, "Improved disturbance detection technique for power-quality analysis," *IEEE Trans. Power Del.*, vol. 26, no. 2, pp. 1286–1287, Apr. 2011.
[24] S. Mishra, C. N. Bhende, and B. K. Panigrahi, "Detection and classification of power quality disturbances using S-transform and probabilistic neural network," *IEEE Trans. Power Delivery*, vol. 23, no. 1, pp. 280–287, Jan. 2008.
[25] B. Gustavsen and A. Semlyen, "Rational approximation of frequency domain responses by vector fitting," *IEEE Trans. Power Del.*, vol. 14, no. 3, pp. 1052–1061, Jul. 1999.
[26] M. S. Sarto, A. Scarlatti, and C. L. Holloway, "On the use of fitting models for the time-domain analysis of problems with frequency-dependent parameters," in *Proc. IEEE EMC Int. Symp. Record. Int. Symp. Electromagn. Compat.*, Aug. 2001, pp. 588–593.

LULU LI (Member, IEEE) received the B.Sc., M.Sc., and Ph.D. degrees in electrical engineering from Chongqing University, Chongqing, China, in 2011, 2014, and 2019, respectively.

From March 2018 to March 2019, she was a Visiting Ph.D. Student with the University of Alberta, Edmonton, AB, Canada. Since August 2019, she has been a Lecturer with the Faculty of Electric Power Engineering, Kunming University of Science and Technology. Her research interests include power disturbance analytics and power cables.

ZONGYUN YANG received the B.S. degree in energy and power engineering from Northeast Electric Power University, China, in 2020. He is currently pursuing the master's degree with the Kunming University of Science and Technology.

His research interests include power disturbance analytics and non-intrusive cable insulation monitoring.

ZHAO LUO (Member, IEEE) received the B.S. degree in electronic science and technology from the Nanjing University of Posts and Telecommunications, China, in 2008, and the M.S. and Ph.D. degrees in electrical engineering from Southeast University, China, in 2013 and 2018, respectively.

He is currently an Associate Professor with the Faculty of Electric Power Engineering, Kunming University of Science and Technology. His research interests include distributed generations, microgrids, and power cables.

KEZHEN LIU received the B.S. degree in power system and automation from the Huazhong University of Science and Technology, China, in 1996, the M.S. degree in water resources and hydraulic engineering from the Kunming University of Science and Technology, China, in 2001, and the Ph.D. degree in power system and automation from the Harbin Institute of Technology, China, in 2013.

She is currently a Professor with the School of Electric Power Engineering, Kunming University of Science and Technology. Her research interests include power system analysis and cable insulation monitoring.